THE JOURNAL OF BIOLOGICAL CHEMISTRY VOL. 283, NO. 29, pp. 20484–20494, July 18, 2008

Functional Consequences of the Human Cardiac Troponin I Hypertrophic Cardiomyopathy Mutation R145G in Transgenic Mice*

Received for publication, February 29, 2008, and in revised form, April 18, 2008 Published, JBC Papers in Press, April 22, 2008, DOI 10.1074/jbc.M801661200

Yuhui Wen[‡], Jose Renato Pinto[§], Aldrin V. Gomes[¶], Yuanyuan Xu[‡], Yingcai Wang[§], Ying Wang[‡], James D. Potter[§1,2], and W. Glenn L. Kerrick[‡1]

From the [‡]Department of Physiology and Biophysics and [§]Department of Molecular and Cellular Pharmacology, University of Miami, Miller School of Medicine, Miami, Florida 33136 and the [¶]Section of Neurobiology, Physiology, and Behavior, University of California, Davis, California 95616

In this study, we addressed the functional consequences of the human cardiac troponin I (hcTnI) hypertrophic cardiomyopathy R145G mutation in transgenic mice. Simultaneous measurements of ATPase activity and force in skinned papillary fibers from hcTnI R145G transgenic mice (Tg-R145G) *versus* hcTnI wild type transgenic mice (Tg-WT) showed a significant decrease in the maximal Ca^{2+}-activated force without changes in the maximal ATPase activity and an increase in the Ca^{2+} sensitivity of both ATPase and force development. No difference in the cross-bridge turnover rate was observed at the same level of cross-bridge attachment (activation state), showing that changes in Ca^{2+} sensitivity were not due to changes in cross-bridge kinetics. Energy cost calculations demonstrated higher energy consumption in Tg-R145G fibers compared with Tg-WT fibers. The addition of 3 mM 2,3-butanedione monoxime at *p*Ca 9.0 showed that there was ~2–4% of force generating cross-bridges attached in Tg-R145G fibers compared with less than 1.0% in Tg-WT fibers, suggesting that the mutation impairs the ability of the cardiac troponin complex to fully inhibit cross-bridge attachment under relaxing conditions. Prolonged force and intracellular [Ca^{2+}] transients in electrically stimulated intact papillary muscles were observed in Tg-R145G compared with Tg-WT. These results suggest that the phenotype of hypertrophic cardiomyopathy is most likely caused by the compensatory mechanisms in the cardiovascular system that are activated by 1) higher energy cost in the heart resulting from a significant decrease in average force per cross-bridge, 2) slowed relaxation (diastolic dysfunction) caused by prolonged [Ca^{2+}] and force transients, and 3) an inability of the cardiac TnI to completely inhibit activation in the absence of Ca^{2+} in Tg-R145G mice.

Hypertrophic cardiomyopathy (HCM)[3] is an autosomal dominant disease characterized by left and/or right ventricular hypertrophy (with left ventricular hypertrophy being dominant) and interstitial fibrosis (1). Patients present symptoms including arrhythmias, severe cardiac dysfunction, and sudden cardiac death (2). HCM is linked to dominant missense mutations in almost all of the genes encoding sarcomeric proteins, including the cardiac troponin (cTn) complex (3–5).

The cTn complex is responsible for regulating cardiac muscle contraction, and it contains three subunits: cardiac troponin C (cTnC), the Ca^{2+}-binding subunit; cardiac troponin I (cTnI), the inhibitory subunit that binds to actin preventing the formation of cross-bridges; and cardiac troponin T (cTnT), which anchors the cTn complex to the thin filament by binding to cTnC, cTnI, and tropomyosin. The cTn complex acts as a Ca^{2+} sensor. When intracellular [Ca^{2+}] increases during the action potential, Ca^{2+} binds to cTnC, which then binds to the C terminus of the cTnI. This binding causes a conformational change in the cTn complex, which releases cTnI from its inhibitory site on actin and changes the position of tropomyosin on the actin filament, thereby activating the actin filaments and leading to muscle contraction (6, 7). When intracellular [Ca^{2+}] is sequestered by the sarcoplasmic reticulum, Ca^{2+} dissociates from cTnC and causes cTnI to bind to actin, inducing muscle relaxation.

Kimura *et al.* (8) reported five missense mutations in cTnI, R145G, R145Q, R162W, G203S, and K206Q, that are associated with HCM. Very little clinical data in humans was available, but a patient reported carrying the hcTnI R145G mutation had typical ventricular hypertrophy (8). Since then, another 15 mutations in cTnI have been reported (3, 9–12). A number of researchers have studied the effects of these HCM-related mutations on actomyosin ATPase and contractility in skinned fibers, cardiomyocytes, and transgenic animals (13–22). Mutations in the inhibitory region of cTnI have been extensively investigated for a decade; especially the hcTnI R145G mutation (positively charged arginine replaced by an uncharged glycine). In an hcTnI R145G-exchanged porcine cardiac myofibril-reconstituted system, Takahashi-Yanaga *et al.* (16, 20) showed no change in the maximal force, whereas Lang *et al.* (14) reported a decrease in the maximum force. At the same time, both of them showed an increase in the Ca^{2+} sensitivity of force devel-

* This work was supported, in whole or in part, by National Institutes of Health Grants HL-67415 and HL-42325. The costs of publication of this article were defrayed in part by the payment of page charges. This article must therefore be hereby marked "*advertisement*" in accordance with 18 U.S.C. Section 1734 solely to indicate this fact.

[1] Joint senior authors who contributed equally to this work.

[2] To whom correspondence should be addressed: 1600 N.W. 10th Ave. (R-189), Miami, FL 33136. Tel.: 305-243-5874; Fax: 305-324-6024; E-mail: jdpotter@miami.edu.

[3] The abbreviations used are: HCM, hypertrophic cardiomyopathy, TnI, tropinin I; cTn, cardiac troponin; cTnI, cardiac troponin I; cTnT, human cardiac troponin T; hcTnI, human cardiac troponin I; BDM, 2,3-butanedione monoxime; NTg, nontransgenic; Tg-WT, hcTnI wild type transgenic mouse; Tg-R145G, hcTnI R145G transgenic mouse.

opment. In the reconstituted actin-tropomyosin-activated myosin ATPase assay, Takahashi-Yanaga *et al.* (16, 20), Lang *et al.* (14), and Elliott *et al.* (15) showed that this specific mutation reduced the ability of cTn to inhibit the actomyosin ATPase activity in the absence of Ca^{2+} and reduced the maximal ATPase activity in the presence of Ca^{2+}. In contrast, Kruger *et al.* (13) found a slightly decreased Ca^{2+} sensitivity of force development in myofibrils from mouse cardiac TnI R146G (mcTnI R146G) transgenic mice but no change in hcTnI R145G-exchanged murine cardiac myofibrils. They also observed a slightly significant upward shift of the passive force-sarcomere length curve at *p*Ca 7.5, which was reversed by the addition of 2,3-butanedione monoxime (BDM) in both reconstituted myofibrils and transgenic mice myofibrils. James *et al.* (21) constructed transgenic mice carrying mcTnI R146G, which showed increased Ca^{2+} sensitivity but did not develop hypertrophy or pathology, except in parous females. However, Sanbe *et al.* (22) found increased Ca^{2+} sensitivity and significant levels of interstitial fibrosis and myocyte disarray even at low protein expression levels in the transgenic rabbit model that carried rabbit cTnI R146G (rcTnI R146G). At high levels of protein expression in this model, the rabbits died prematurely.

Unlike previous reports, in this study the physiological function of the human cardiac TnI (hcTnI) R145G mutation was measured in transgenic mice expressing the hcTnI R145G (Tg-R145G) compared to transgenic mice expressing hcTnI wild type (Tg-WT). Using skinned papillary fiber preparations, the cross-bridge turnover rate, energy cost (ATPase/force), and cross-bridge attachment in the absence of Ca^{2+} were measured. The hcTnI R145G mutation had no effect on the rate of dissociation of force-generating cross-bridge as a function of the activation state (number of cross-bridges attached in the presence of Ca^{2+}) but caused a significant decrease in average force/cross-bridge, an increase in Ca^{2+} sensitivity of force development and ATPase activity, and a decrease in cooperativity of thin filament activation (decrease in the slope of the force-*p*Ca relationship). A slight increase in cross-bridge attachment at *p*Ca 9.0 was observed in Tg-R145G skinned fibers that were abolished by the addition of 3 mM BDM. In contrast to previous studies, the intracellular Ca^{2+} and force transients were evaluated in intact papillary muscle, and an increase in the duration of both force and intracellular Ca^{2+} transients was observed. As discussed below, all of these physiological findings suggest that the hcTnI R145G mutation would cause both systolic and diastolic dysfunction and may explain the poor prognosis for patients with this mutation.

MATERIALS AND METHODS

Generation and Characterization of Transgenic Mice

Transgene Construction and Transgenic Mice Generation—The wild type (WT) cDNA for human cardiac TnI (hcTnI) was obtained by reverse transcription-PCR using total RNA isolated from human cardiac ventricle and cloned into the pET-3d vector (Novagen) at NcoI/BamHI sites. The hcTnI R145G mutation was made by using overlapping sequential PCR (23) and cloned into the same vector as hcTnI WT. The WT and R145G cDNAs were released from pET-3d and subcloned into the SalI site of the plasmid, α-myosin heavy chain promoter (a gift from Dr. J. Robbins, Cincinnati Children's Hospital Medical Center). The resulting constructs contained about 5.5 kb of the mouse α-myosin heavy chain promoter, including the first two exons and part of the third, followed by WT/R145G-cDNA and a downstream 630-base pair region of the 3′-untranslated region of the human growth hormone. The transgene construct described above was digested with NotI to release a 7-kilobase fragment that was used for microinjection. This fragment was purified by agarose gel electrophoresis, followed by electroelution and resuspension in 10 mM Tris-HCl, pH 7.4, 0.1 mM EDTA at a final concentration of 20 μg/ml. Mouse pronuclei were injected, and the surviving embryos were implanted using standard methods (24). Founder mice were identified by preparing tail clip DNA and analyzing their PCR products corresponding to the α-myosin heavy chain promoter and Arg^{192} residue in the cTnI. Stable transgenic lines were generated by breeding founders to nontransgenic (NTg) B6SJL mice. The hcTnI transgenes were confirmed by standard PCR using a pair of primers specifically amplifying a 600-bp fragment of the hcTnI of the transgenic construct. Each PCR also included a set of primers specific for the mouse actin gene to confirm successful genomic amplification (eliminating false negative animals and producing a 200-bp PCR product). Two lines of Tg-WT and Tg-R145G (Fig. 1*b*) were produced, and the line with higher protein expression was used for histopathology and skinned and intact fiber studies.

Analysis of Protein Expression—The expression of hcTnI protein in the transgenic mice was determined by Western blot analysis. The experimental mouse heart and control human heart tissues were minced in a solution of 1% (v/v) β-mercaptoethanol, 1% (w/v) SDS, 1 mM phenylmethylsulfonyl fluoride, 1 mM EDTA, and protease inhibitor mixture (Sigma). These samples were homogenized in 20 mM Tris-HCl, pH 7.4, 1% SDS, 1% β-mercaptoethanol, 10% glycerol on ice, and the total protein concentration of each cleared homogenate was determined by the Bio-Rad Coomassie Plus assay. SDS-polyacrylamide gels (15%) were run with a total of 2 μg of protein for each lane. Protein was then transferred to nitrocellulose membranes (Bio-Rad). The membrane was blocked in Rockland blocking buffer for 30 min at room temperature. A monoclonal antibody 6F9 (Fitzgerald Industries international Inc.) was used at a 1:4000 dilution for 1 h to detect both human and mouse cTnI. The gel mobility of hcTnI is faster than that of mice due to its lower molecular mass (24 kDa *versus* 25 kDa, respectively). Immunoreactivity was detected using goat anti-mouse IgG antibody labeled with CY5.5 fluorescent dye at a 1:3000 dilution for 1 h at room temperature, the reaction signal blot was scanned with an Odyssey Infrared Imager (LICOR), and analysis was carried out on a Dell Pentium computer using Scion Image software. The percentage of transgenic protein expression was calculated as (transgenic human TnI/(endogenous mouse TnI + transgenic TnI)) × 100.

Histopathological Characterization

After euthanasia, the hearts of mice from NTg, Tg-WT, and Tg-R145G were excised, weighed, and immersed in 10% (v/v) buffered formalin. Slides of whole hearts were prepared by

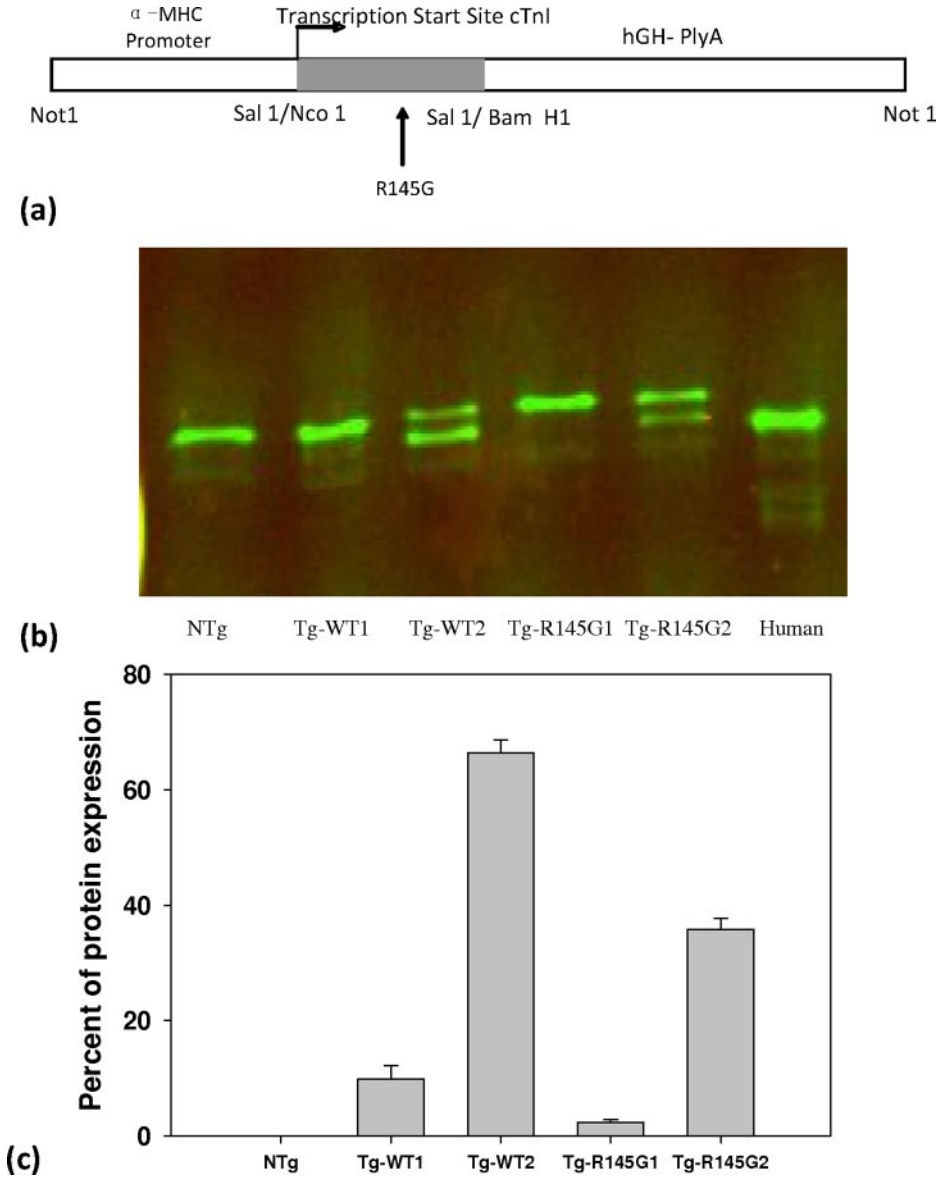

FIGURE 1. *a*, hcTnI transgene construct; a schematic diagram of the hcTnI transgene to generate hcTnI R145G-overexpressing mice. Sequences corresponding to the α-myosin heavy chain (MHC) promoter/enhancer sites are shown as *open boxes*. The sequence corresponding to the hcTnI cDNA is represented as a *gray box*. The point mutation introduced in the hcTnI cDNA, relevant restriction sites, and transcription start site are indicated. *b*, Western blots of heart extracts from Tg-WT and Tg-R145G lines *versus* NTg and human heart extraction. The protein expression levels in transgenic mice were assessed on the basis of densitometry. Western blots were labeled with monoclonal troponin I 6F9 antibody and followed by a goat anti-mouse secondary antibody. *c*, summary of all generated lines for Tg-WT and Tg-R145G. Two lines of Tg-WT-express 9.84% ± 2.37 and 66.4% ± 2.26% mutant protein compared with the whole cTnI amount in mouse heart. Two lines of Tg-R145G express 2.34% ± 0.47 and 35.8% ± 2.0% mutant protein compared with the whole cTnI amount in mouse heart. The results are the mean ± S.E. of five measurements.

American Histolabs, Inc. (Gaithersburg, MD). The paraffin-embedded, longitudinal sections of whole hearts stained with hematoxylin and eosin and Masson's trichrome were examined for overall morphology, hypertrophy, myofilament disarray, and fibrosis, using a Zeiss microscope and ×40/0.65 Plan Apos objective (Fig. 2). The heart weight/body weight ratio was calculated for all sacrificed mice.

Functional Studies in Skinned Papillary Muscle Fibers

Simultaneous Force and ATPase Measurements—Mouse papillary muscles, ~1 mm long and 60–90 μm in diameter, were dissected from excised mouse heart in relaxing solution and then skinned in relaxing solution containing 1% (v/v) Triton X-100 for 30 min at room temperature. Standard solution contained 85 mM K^+, 2 mM $MgATP^{2-}$, 1 mM Mg^{2+}, 7 mM EGTA, 10^{-9} or $10^{-3.4}$ M Ca^{2+}, and propionate as the major anion. Ionic strength was adjusted to 0.15, and pH was maintained at 7.00 ± 0.02 with imidazole propionate. Relaxing solutions were solutions with no added Ca^{2+}. Maximal contracting solutions were solutions that gave maximal tension beyond which increasing Ca^{2+} further does not increase tension. For ATPase measurements, solutions contained, in addition to the constituents described above, 5 mM phosphoenolpyruvate, 0.4 mM NADH, 100 units/ml pyruvate kinase, and 140 units/ml L-lactic dehydrogenase. The concentrations of the various ionic species were determined by a computer program using binding constants from the literature (25). The Ca^{2+} concentration in the cuvette perfusing the skinned preparation was varied by use of a gradient maker (Scientific Instruments GmbH, Heidelberg) to mix two solutions of known Ca^{2+} and ionic composition together. A complete description of the method has been given by Allen *et al.* (26). The Ca^{2+} concentration in the cuvette perfusing the skinned preparation was varied continuously from *p*Ca 9 to *p*Ca 3.4. The fluorescent Ca^{2+} indicator Calcium Green-2 (Molecular Probes) was used to calibrate and calculate the [Ca^{2+}] during measurements. Calcium Green-2 changes its fluorescence over the range of [Ca^{2+}] required for activation of contraction and ATPase activity. The K_d of Calcium Green-2 used to calculate *p*Ca was $10^{-5.53}$ M. The concentration of Calcium Green-2 in the gradient solution was 1.0 μM. The Calcium Green-2 fluorescence was excited at 480 nm, and the fluorescence was measured with a cut-off filter at 515 nm.

The skinned fibers were placed in a quartz cuvette and mounted in the Guth Muscle Research System (skinned fibers are held in stainless steel clips attached to a force transducer at one end and a linear motor on the other end) (27), which allowed for simultaneous measurements of force and ATPase (28–30). The sarcomere length of the fibers was set by removing the slack from the fiber and stretching the fiber 10%. The solution in the cuvette was changed

TABLE 1

Heart weight/body weight ratios (R) in Tg-R145G *versus* Tg-WT and NTg

G, gender; H, heart weight; B, body weight; R, H/B. M, male; F, female. NTg controls are from the littermates of the R145G transgenic line 2. The average ratios (R) are means of n experiments ± S.E. None of the differences between NTg, Tg-WT, and Tg-R145G are statistically significant ($p > 0.05$).

NTg (R_{av} = 4.82 ± 0.21; n = 12)					Tg-WT (R_{av} = 5.37 ± 0.18; n = 13)					Tg-R145G (R_{av} = 5.12 ± 0.23; n = 16)				
Age	G	H	B	R (× 10^{-3})	Age	G	H	B	R (× 10^{-3})	Age	G	H	B	R (× 10^{-3})
months		*g*	*g*		*months*		*g*	*g*		*months*		*g*	*g*	
1.5	F	0.110	27.43	4.01	1.0	F	0.103	18.41	5.60	1.0	F	0.129	18.40	7.03
2.5	F	0.070	16.73	4.20	1.0	M	0.109	21.59	5.05	2.5	F	0.079	16.22	4.90
4.0	F	0.186	20.38	5.05	2.0	M	0.119	22.41	5.31	3.0	M	0.104	20.34	5.10
4.3	M	0.109	20.98	5.20	2.7	M	0.107	24.91	4.30	4.0	M	0.118	23.87	4.96
5.0	M	0.123	19.37	6.35	3.0	F	0.111	21.78	5.10	4.5	M	0.108	22.16	4.87
5.0	F	0.099	19.74	5.01	3.0	F	0.148	22.15	6.68	4.8	M	0.109	21.59	5.03
5.3	F	0.083	21.38	3.88	3.1	F	0.103	22.49	4.58	5.0	M	0.126	26.41	4.77
7.0	M	0.183	38.72	4.73	3.2	F	0.135	23.187	6.08	5.0	F	0.133	28.67	4.64
10.0	M	0.189	32.73	5.77	4.0	F	0.125	22.82	5.48	6.1	F	0.195	34.68	5.65
11.0	F	0.186	38.95	4.78	4.2	F	0.119	21.57	5.52	7.0	F	0.153	30.15	5.08
11.0	M	0.127	27.34	4.63	4.3	M	0.135	22.79	5.92	9.8	F	0.108	29.95	3.59
15.0	F	0.114	27.13	4.21	10.0	F	0.176	36.05	4.87	10.0	M	0.160	33.48	4.76
					11.5	M	0.169	33.77	5.01	12.1	F	0.117	30.49	3.84
										15.0	F	0.137	29.28	4.68
										15.0	M	0.282	40.57	6.96
										18.0	F	0.218	36.43	5.99

every 20 s using a peristaltic pump triggered by a computer. The hydrolysis of ATP was measured by the NADH fluorescence method, in which ATP is regenerated from ADP and phosphoenolpyruvate by the enzyme pyruvate kinase (27, 31). This reaction was coupled to the oxidation of NADH (fluorescent) to NAD (nonfluorescent) and the reduction of pyruvate to lactate by L-lactic dehydrogenase (27, 29, 31). In this reaction, 1 mol of phosphoenolpyruvate and NADH was used to produce 1 mol of ATP and NAD. The solution surrounding the fiber in the quartz cuvette was illuminated at 340 nm, and the decrease in NADH concentration was detected by a decrease in the fluorescence signal $\lambda = 450$ nm. The solution in the cuvette was changed every 20 s, and the fluorescence change taking place between each solution change was converted to the rate of ATP hydrolysis by comparison with NADH standards. The force and ATPase activity were plotted as a function of *p*Ca. Each *curve* is the averaged data, as shown in Fig. 3.

Fraction Cross-bridge Attachment at Maximal Ca^{2+} Activation—At the end of each experiment, the substitution of 10 mM MgADP for 2 mM ATP was made to the maximal Ca^{2+}-activating solution in the cuvette perfusing the fiber. This substitution forces all cross-bridges into the force generating state producing the maximal force that the fiber can develop. The maximal Ca^{2+} activated force is then divided by the maximum force the muscle can develop in the presence of 10 mM MgADP. This ratio is the fraction cross-bridge attachment at maximal Ca^{2+} activation, as shown in Fig. 5.

Measurements of the Rate of Cross-bridge Detachment (g)—The force that a muscle develops can be characterized by the apparent rate for the formation of force generating states (f) and the dissociation of force-generating rate (g) according to the two-state model of Huxley, as shown in Scheme 1 (32).

$$\text{Nonforce} \underset{g}{\overset{f}{\rightleftharpoons}} \text{Force}$$

SCHEME 1

Based on this kinetic scheme, g can be calculated by Equation 1,

$$g = \text{ATPase/total cross-bridges attached} \quad \text{(Eq. 1)}$$

where total cross-bridges attached = [myosin subfragment 1 head] × fractional of cross-bridge attachment at any Ca^{2+} concentration. The fractional of cross-bridge attachment at any Ca^{2+} concentration equals the fractional cross-bridge attachment at maximal Ca^{2+} activation times the normalized force. The total intracellular myosin subfragment 1 head concentration in muscle is ~154 μM (33). In this study, g was calculated based on the above equation. Fig. 6 illustrates g as a function of normalized force.

Force-Stretch Relationship Measurements in Skinned Papillary Muscle at Low Ca^{2+} Concentration—The mouse papillary muscle was skinned and mounted as described above. After mounting the fiber, it was continuously perfused with the relaxing solution (*p*Ca 9.0 solution). Once mounted in the tweezers, the slack in the fiber was removed. The force measurement at this point was set as zero. The fiber was then stretched 10% of its original length. When the steady state force was established, data points were recorded as shown in Fig. 8*a*. Each point was taken at 10-s intervals. After several data points were collected, the *p*Ca 9.0 perfusing solution in the cuvette was changed to *p*Ca 9.0 with 3 mM BDM solution, and force data were again recorded. Without changing the solution, the fiber was stretched to 20% of its original length. After the force reached the steady state, we again recorded the steady state force before changing the *p*Ca 9.0 3 mM BDM solution to the *p*Ca 9.0 minus BDM solution. The procedure was repeated at the 30 and 40% stretch of its original length. After 40% stretch, we released fiber to its original length and changed the solution to maximum activating *p*Ca 3.4 solution to contract the fiber. We normalized the force at each stretch to the maximum force the fiber can develop at *p*Ca 3.4.

Functional Studies in Intact Papillary Muscle Fibers; Measurements of [Ca^{2+}] and Force Transients

Following CO_2 euthanasia, hearts were removed quickly and soaked in ice-cold saline (0.9% NaCl). Intact papillary muscle was dissected quickly from right ventricles in oxygenated Krebs-Henseleit solution (119 mM NaCl, 4.6 mM KCl, 11 mM glucose, 25 mM $NaHCO_3$, 1.2 mM KH_2PO_4, 1.2 mM $MgSO_4$,

1.8 mM $CaCl_2$) containing 30 mM 2,3-butanedione monoxime and mounted in the Guth muscle research system (29). Fibers were loaded in oxygenated Krebs-Henseleit solution without 2,3-butanedione monoxime for 1 h at room temperature to allow the muscle to adapt to the extracellular environment. The fibers were then loaded with 5 μM Fura-2/AM for 1 h at room temperature in oxygenated Krebs-Henseleit solution containing 0.5% (v/v) Cremophor, which increases the solubility of Fura-2 AM. The muscle was stimulated at 1.0 Hz through the two tweezers attached to the ends of the preparation. Once the preparation was mounted in the apparatus, muscle length was adjusted until maximum active twitch force was obtained. Force and fluorescence corresponding to either 340 or 380 nm excitation were recorded by the computer. The fluorescence 340 nm/380 nm ratio was calculated and plotted along with force. The force and calcium transients were normalized and then averaged and plotted as a function of time, as shown in Fig. 9.

Statistical Analysis

Data are expressed as the average of n experiments ± S.E. Statistically significant differences were determined using an unpaired Student's t test (Sigma Plot 8.0), with significance defined as follows: *, $p < 0.05$; **, $p < 0.01$.

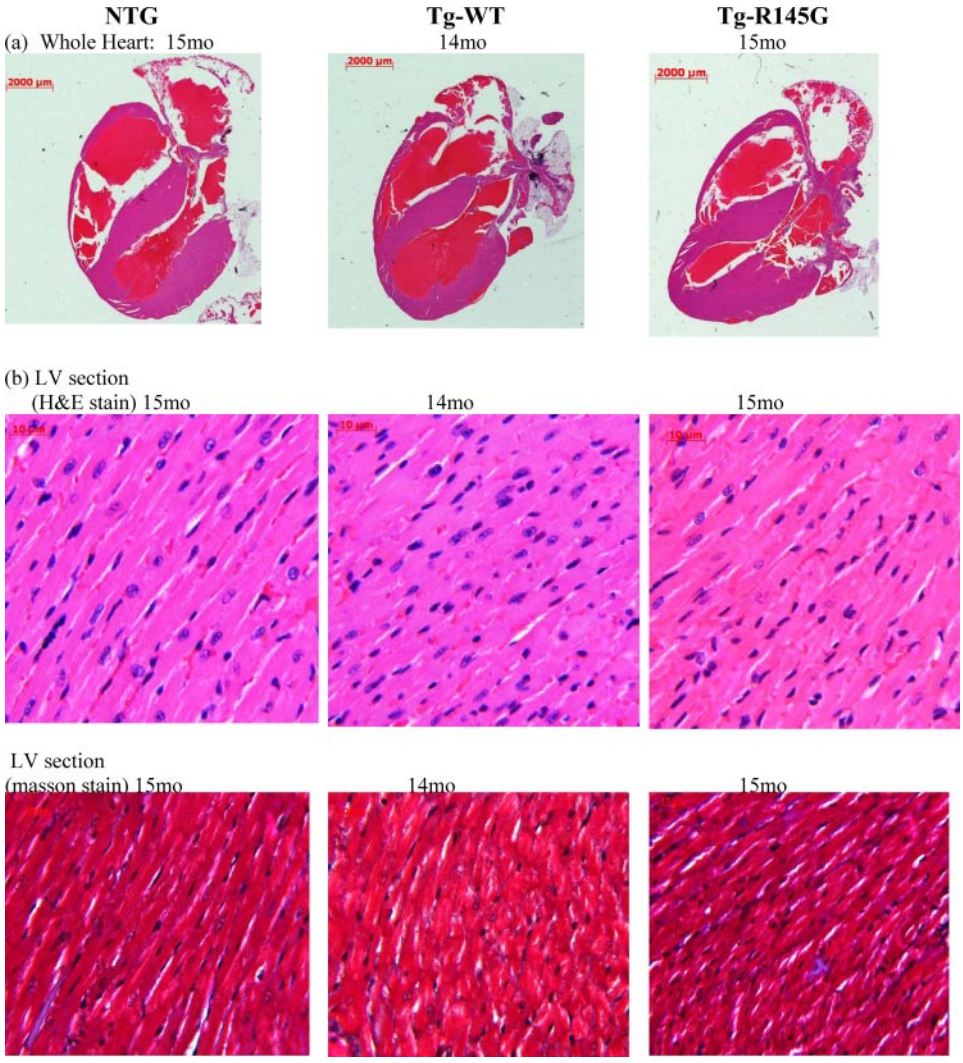

FIGURE 2. **Microscopic view of transgenic mouse hearts stained with hematoxylin and eosin (*H&E*) and Masson's trichrome.** *a*, the hematoxylin and eosin stain of longitudinal section of whole mouse heats of 14–15-month-old NTg and Tg-WT *versus* Tg-R145G. Shown is a microscopic view of left ventricular (*b*) and septal sections (*c*) of Tg-R145G *versus* NTg and Tg-WT, stained with hematoxylin and eosin (*top*) and Masson's trichrome (*bottom*). *d*, the hematoxylin and eosin stain of papillary muscle of Tg-R145G *versus* NTg and Tg-WT. *Scale bar*, 2000 μm in *a* and 10 μm in *b–d*. *mo*, age in months; *LV*, left ventricle sections; *SP*, septal sections.

RESULTS

Generation and Characterization of Tg-WT and Tg-R145G

The expression of hcTnI WT and R145G proteins were driven by the α-MHC promoter in the mouse heart (Fig. 1*a*). The WT and mutant protein expression level were assessed on the basis of gel densitometry (Fig. 1*b*). The hcTnI WT and R145G protein expressions were normalized to total cTnI content. The human cTnI replaced the murine cTnI in the heart, so the murine cTnI was reduced. Two lines of Tg-WT were generated, expressing ~10% (L1) and ~65% (L2) of hcTnI compared with the whole cTnI amount in mouse heart. Additionally, two lines of Tg-R145G were produced, expressing ~2% (L1) and ~35% (L2) mutant protein (Fig. 1, *b* and *c*). This method has been used successfully in our laboratory (34). Line 2 of the Tg-WT and line 2 of the Tg-R145G consistently produced the expected transgene product levels and were chosen for further histopathology and functional studies.

Histopathology Studies

The heart weight/body weight ratios in relation to age increase of the mice were evaluated. No statistically significant difference between NTg, Tg-WT, and Tg-R145G was observed (Table 1). The heart tissue morphology of NTg, Tg-WT, and Tg-R145G is presented in Fig. 2. Fig. 2*a* shows the hematoxylin and eosin staining of longitudinal sections of whole mouse hearts of 14–15-month-old NTg and Tg-WT *versus* Tg-R145G. There were no significant differences seen in the whole heart sections from Tg-R145G compared with that of NTg and Tg-WT. Fig. 2, *b* and *c*, shows the left ventricular wall and septal sections of these hearts stained with hematoxylin and eosin (*top*) and Masson's trichrome (*bottom*), respectively. No myocyte disarray (hematoxylin and eosin) or fibrosis (Masson's stain) was found in both the left ventricle and septum of Tg-R145G when compared with control mice. As shown in Fig. 2*d*, the papillary muscles of these mice showed no myofibrillar disarray compared with NTg and Tg-WT littermates.

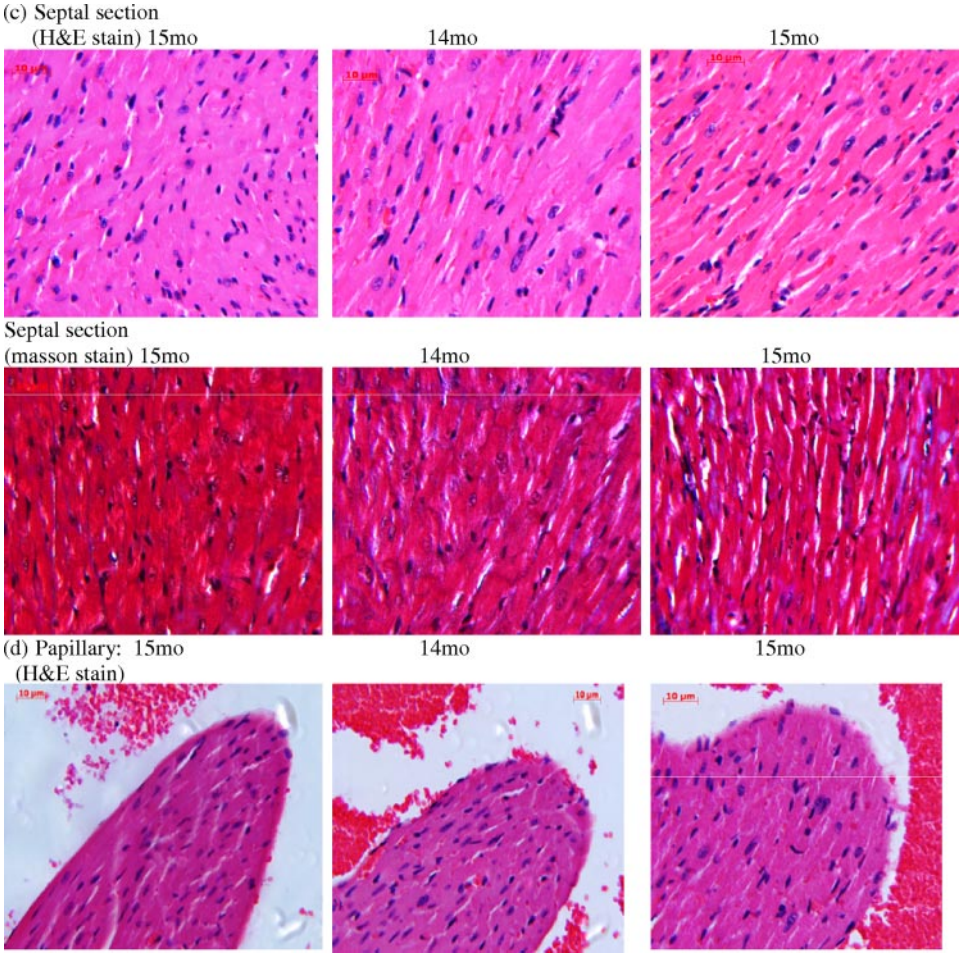

FIGURE 2—*continued*

Functional Studies

Skinned Papillary Muscle Fibers—Simultaneous ATPase-*p*Ca and force-*p*Ca measurements were performed in freshly skinned papillary muscle fibers from all groups of transgenic *versus* control mice under isometric conditions. In both skinned and intact fiber experiments, 3–7-month-old mice were used. Measurements were also performed with 12.0 + 1.0-month-old mice. No differences in functional studies were observed between these different age groups. An increased Ca^{2+} sensitivity in the Tg-R145G fibers compared with Tg-WT fibers was seen in steady-state force development measurements with $pCa_{50} = 5.264 \pm 0.02$ ($n = 10$) and $pCa_{50} = 5.157 \pm 0.017$ ($n = 13$) for Tg-R145G and Tg-WT, respectively. The $\Delta pCa_{50} = 0.107$ was statistically significant ($p < 0.05$). The Hill coefficient of force in Tg-R145G fibers ($n_H = 1.8617 \pm 0.144$) was significantly lower than that in Tg-WT fibers ($n_H = 2.518 \pm 0.115$) (Fig. 3*a*). Fig. 3*b* showed that the Ca^{2+} sensitivity measured by ATPase activity was also increased in Tg-R145G fibers compared with Tg-WT fibers. The pCa_{50} was 5.5793 ± 0.022 ($n = 10$) and 5.3819 ± 0.02 ($n = 13$) for Tg-R145G and Tg-WT fibers, respectively. The $\Delta pCa_{50} = 0.1974$ between Tg-R145G and Tg-WT fibers was statistically significant ($p < 0.05$). As expected, there was no significant difference in pCa_{50} and Hill coefficient between the Tg-WT and NTg fibers as shown in Fig. 3, *c* and *d*. In Fig. 4, maximal force values (10^5 newtons/m^2) and maximal ATPase rates (s^{-1}/myosin S1 head) were presented for NTg, Tg-WT, and Tg-R145G skinned fibers. As shown, there was an ~14% decrease in maximal Ca^{2+} activated force between Tg-R145G fibers (0.6032 ± 0.03) and Tg-WT fibers (0.6902 ± 0.023) (Fig. 4*a*). No significant differences were observed in the fraction of cross-bridges attached at maximum Ca^{2+} in all groups of fibers (see "Materials and Methods" for details) (Fig. 5). There was no statistically significant difference in maximal ATPase activity between Tg-WT fibers (5.3275 ± 0.241) and Tg-R145G fibers (5.2937 ± 0.210) (Fig. 4*b*). No significant difference was observed comparing the maximal Ca^{2+}-activated force and maximal ATPase rates between NTg and Tg-WT fibers (Fig. 4).

As illustrated in Fig. 6, the rate of cross-bridge turnover (*g*) as a function of activation state (fraction of maximum activated force) was the same in all groups of fibers. These results show that the R145G HCM mutation does not affect the turnover rate of the cross-bridge at Ca^{2+}-activating levels.

The energy cost in Tg-R145G, Tg-WT, and NTg fibers was investigated by using ATPase activity divided by force in all groups of fibers. As shown in Fig. 7, energy cost (ATPase/force) as a function of activated state in Tg-R145G skinned fibers is statistically significantly higher than that in Tg-WT and NTg skinned papillary fibers.

To investigate the inhibition of cross-bridge cycling in the absence of Ca^{2+} ($pCa = 9.0$), we stretched the skinned fiber over a range of muscle lengths (10–40%) at *p*Ca 9.0 with or without 3 mM BDM and recorded the force. Fig. 8*a* is representative of two independent experiments in Tg-WT and Tg-R145G fibers (see "Materials and Methods" for details). Fig. 8*b* showed a slight increase in the relative force (force normalized to the maximum force at the *p*Ca 3.4) in Tg-R145G compared with the Tg-WT during stretch. The addition of 3 mM BDM at *p*Ca 9.0 decreased this relative force to a level similar to Tg-WT. In Fig. 8*c*, the relative force differences between the presence and absence of BDM in Tg-WT and Tg-R145G fibers were shown at each stretch. The relative force differences between ±BDM in Tg-R145G fibers at each stretch showed a statistically significant higher number of cross-bridges attached (~2–4% of the maximum cross-bridge attachment) than that in Tg-WT fibers (less than 1% of the maximum cross-bridge attachment), meaning that the hcTnI R145G mutation caused incomplete inhibition of activation under relaxing conditions ($pCa = 9.0$).

Intact Papillary Muscle Fibers—In another series of experiments, simultaneous force and $[Ca^{2+}]$ transient measurements were performed in electrically stimulated intact papillary muscles (Fig. 9 and Table 2). Intact papillary muscles from Tg-R145G, Tg-WT, and NTg were examined for both force and $[Ca^{2+}]$ transients. The muscles were stimulated at 1.0 Hz and the force as well as the fluorescence signals were recorded simultaneously (see "Materials and Methods" for details). Fig. 9 shows the normalized force and $[Ca^{2+}]$ transients for all groups of intact fibers as a function of time in milliseconds. Table 2 summarizes the t_{50} and t_{10} values in milliseconds from the peak to 50 and 10% of force and $[Ca^{2+}]$ during relaxation, respectively. The force transient (Fig. 9*a*) and the $[Ca^{2+}]$ transient (Fig. 9*b*) were significantly prolonged in Tg-R145G compared with Tg-WT and NTg. The t_{50} and t_{10} values for the force transients were ~1.7- and ~2.0-fold longer in the Tg-R145G papillary muscles compared with those of Tg-WT, respectively (Table 2). At the same time, the t_{50} and t_{10} values of the $[Ca^{2+}]$ transient in Tg-R145G papillary muscles were both ~28% longer than that in Tg-WT papillary muscles (Table 2). As expected, Tg-WT and NTg fibers had no change in their force or $[Ca^{2+}]$ transients (Fig. 9, *c* and *d*).

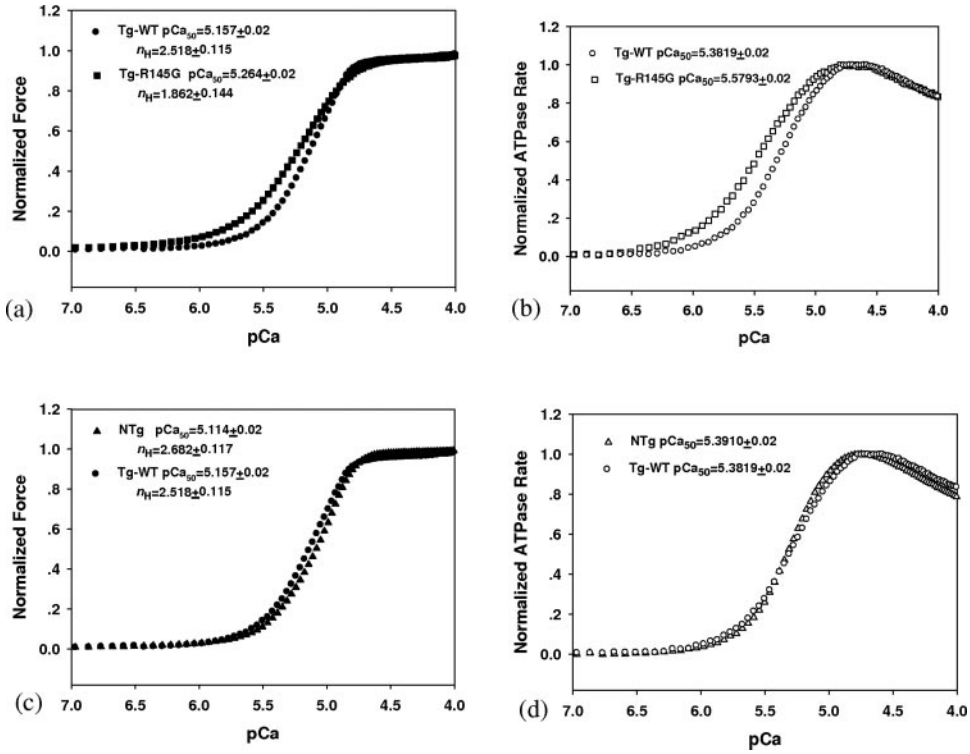

FIGURE 3. **The effects of hcTnI R145G mutation on the Ca^{2+} sensitivity of steady-state force and the ATPase activity were measured simultaneously in isometric muscle fibers.** *a* and *c*, the force-*p*Ca relationship in Tg-R145G ($n = 10$) *versus* Tg-WT ($n = 13$) and NTg ($n = 11$) *versus* Tg-WT ($n = 13$) fibers, respectively. *b* and *d*, the ATPase-*p*Ca relationship between Tg-R145G ($n = 10$) *versus* Tg-WT ($n = 13$) and NTg ($n = 11$) *versus* Tg-WT ($n = 13$) fibers, respectively. The *p*Ca values and Hill coefficients for force curve and *p*Ca values for ATPase curve are shown. Data are expressed as mean of *n* experiments ± S.E.

DISCUSSION

To elucidate the potential mechanisms by which the hcTnI R145G mutation results in ventricular and/or septal hypertrophy and alters cardiac muscle contraction in humans, transgenic mice overexpressing hcTnI R145G in the murine heart were generated. As we can see in Fig. 2*a*, the morphology of hematoxylin and eosin-stained longitudinal sections showed that there were no apparent morphological changes in Tg-R145G, Tg-WT, or their NTg littermates. Also, no difference was seen in the heart weight/body weight ratios in the Tg-R145G mice compared with NTg and Tg-WT. Since no solid evi-

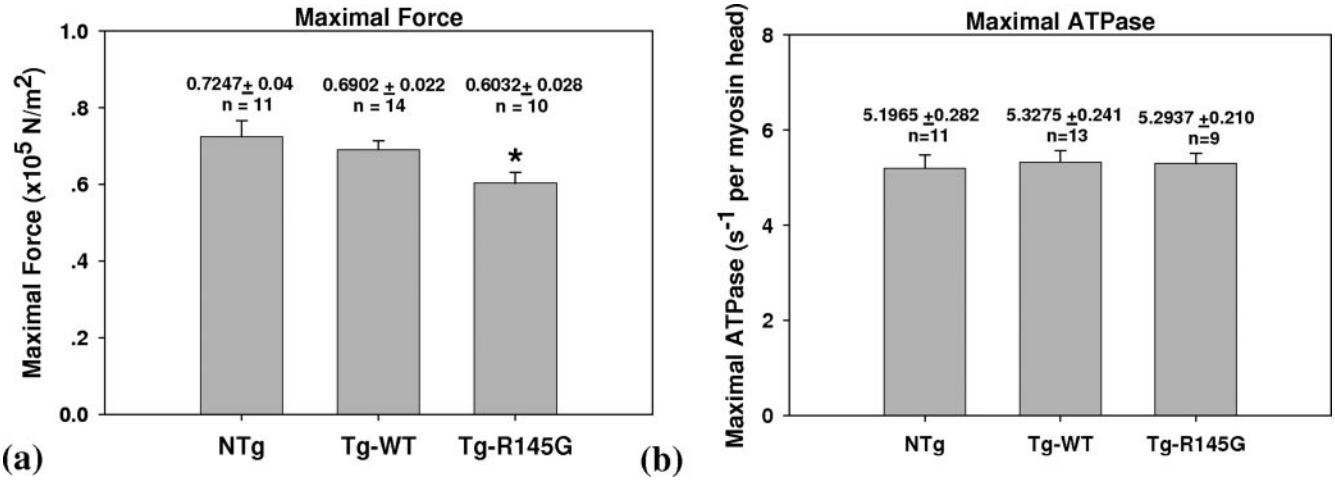

FIGURE 4. **The effect of hcTnI R145G mutation on maximal force (10^5 newtons/m^2) and maximal ATPase activity (s^{-1}/myosin head) in transgenic papillary muscle fibers, respectively.** *a*, the maximal force was ~14% lower in Tg-R145G fibers ($n = 10$) than in Tg-WT fibers ($n = 14$). *b*, there is no significant difference in maximal ATPase in Tg-R145G fibers ($n = 9$) compared with Tg-WT fibers ($n = 13$) ($p > 0.05$). There was no statistically significant difference in both maximal force and ATPase between NTg and Tg-WT fibers ($p > 0.05$). *, statistically significant difference ($p < 0.05$). Data are expressed as mean of *n* experiments ± S.E.

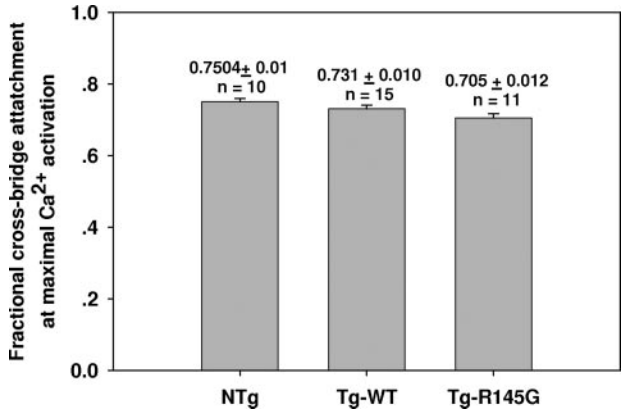

FIGURE 5. **Fractional cross-bridge attachment at maximal Ca^{2+} activation.** Shown is the ratio of the maximal Ca^{2+}-activated force at 2 mM ATP divided by the maximal force the fiber can develop in the presence of 10 mM MgADP in all groups of skinned papillary fibers. There are no significant differences in all groups of fibers ($p > 0.05$). Data are expressed as mean of *n* experiments ± S.E.

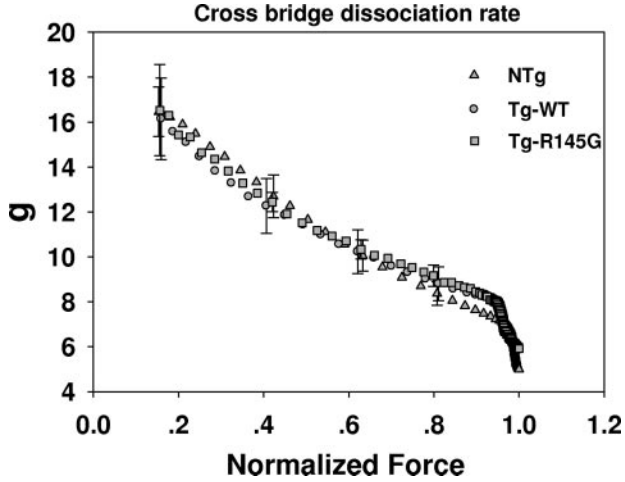

FIGURE 6. **The rate of cross-bridge turnover (*g*) as a function of activation state (fraction of maximum activated force) in transgenic skinned papillary fibers.** As shown, the dissociation of cross-bridge rate (*g*) was the same in Tg-R145G ($n = 10$), Tg-WT ($n = 13$), and NTg ($n = 11$) fibers. Data are expressed as mean of *n* experiments ± S.E.

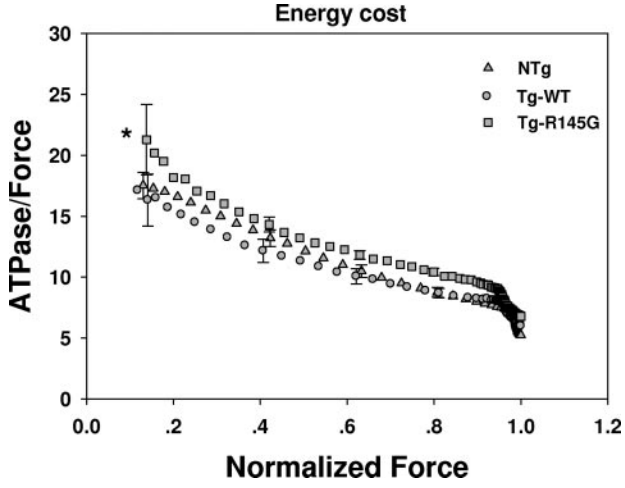

FIGURE 7. **The energy cost (ATPase/force) as a function of activated state (fraction of maximum activated force) in all groups of skinned papillary fibers.** As shown, the Tg-R145G ($n = 10$) fiber has statistically significant higher energy cost (ATPase/force) than that in Tg-WT ($n = 13$) and NTg ($n = 11$) fibers. Statistically significance is defined as follows: *, $p < 0.05$. Data are expressed as mean of *n* experiments ± S.E.

dence was found for fibrosis in the left ventricle and septum based on Masson's trichrome stain, no biochemical tests beyond histology were performed (*i.e.* hydroxyproline content). James *et al.* (21) showed no discernible pathology at any age of α-myosin heavy chain promoter-driven $mcTnI_{R146G}$ mice that had 40% transgenic protein expression, which is in agreement with our findings that no myofibrillar disarray (hematoxylin and eosin stain) or fibrosis (Masson's stain) were observed (Fig. 2). In contrast, only 25% replacement of transgenic protein in a β-myosin heavy chain promoter-driven rabbit cTnI-R146G model showed significant levels of interstitial fibrosis and myocyte disarray (22). The ratio between α-myosin heavy chain and β-myosin heavy chain in the mice is 16:1 (35) compared with 1:4 in rabbits (36). Krenz and Robbins (37) showed that increasing the ratio of β- to α-myosin heavy chain is disadvantageous to mouse and human hearts under severe cardiovascular stress (37). Also, Metzger and co-workers (38) demonstrated that the β-myosin heavy chain is a negative inotrope. They found that the gene transfer-based replacement of α- with β-myosin heavy chain attenuated contractility in a dose-dependent manner (38).

Although hypertrophy was not found in our transgenic model, we know that the functional properties between mouse and human hearts are significantly different. For example, mouse hearts are much smaller and have a much faster heart rate. Second, there are a number of troponin mutations that have distinct phenotypes in humans that are not seen in transgenic mouse models. Third, according to the literature, other laboratories have shown that the higher the expression of mutant proteins, the more likely the murine heart will develop morphological changes. James *et al.* (21) reported that the mcTnI-R146G transgenic mice that displayed mutant protein expression levels of over 50% have apparent phenotypes. Finally, in the case of diastolic dysfunction, the phenotype may only occur when the diastolic dysfunction is severe enough that the heart can no longer adjust stroke volume to accommodate for the diastolic dysfunction, and then hypertrophy may develop. What makes this study unique is that it used transgenic mice expressing both the hcTnI R145G mutation and the proper control hcTnI WT. In this study, using Tg-R145G *versus* Tg-WT made it possible to extend our knowledge to what effects the hcTnI R145G mutation has on physiological function. Other unique aspects of this study are that it used simultaneous force and actomyosin ATPase measurements in the skinned papillary fibers and simultaneous force and Ca^{2+} transient measurements in the intact papillary fibers. Since force is proportional to the number of force-generating cross-bridges attached and ATPase is proportional to cross-bridge turnover rate (32), the simultaneous force and ATPase measurements in skinned fibers make it possible to calculate the rate of cross-bridge turnover, energy cost, and average force per cross-bridge. In addition, simultaneous measurements of intracellular Ca^{2+} and force transients in intact papillary muscles allowed for further observations of changes in physiological function caused by the hcTnI R145G mutation that causes HCM in humans.

Our previous study (14) showed that the hcTnI R145G mutation impaired the ability of TnI to inhibit the ATPase activity in

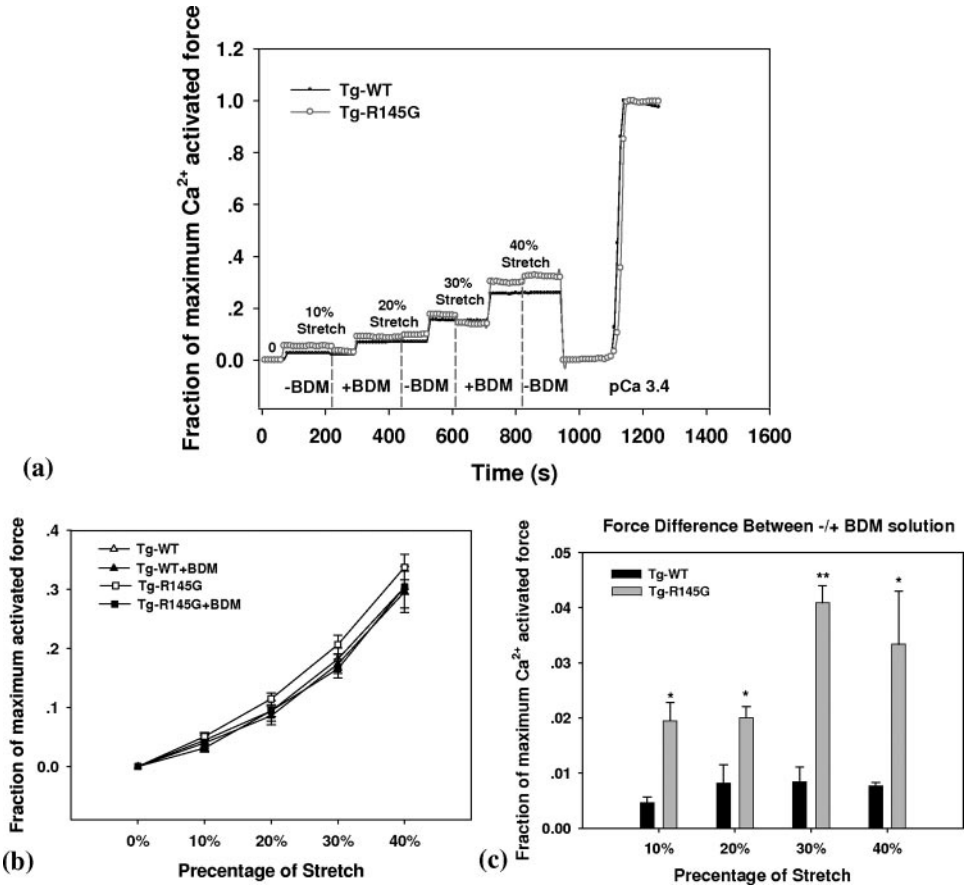

FIGURE 8. **The force of skinned fibers due to different stretch levels at the resting condition with/without 3 mM BDM (see "Materials and Methods" for details).** *a*, a representative experiment for both Tg-WT and Tg-R145G fibers. Force at each stretch was normalized to the maximum Ca^{2+}-activated force at *p*Ca 3.4. The *dashed lines* are the breaking point to change the *p*Ca 9.0 solution with or without 3 mM BDM at each stretch. *b*, Tg-WT ($n = 5$) *versus* Tg-R145G ($n = 3$) force due to fiber stretch in the presence and absence of 3 mM BDM. *c*, force differences between the presence and absence of BDM in fibers at each stretch. Differences in Tg-WT fibers and Tg-R145G fibers are shown in *black* and *gray bars*, respectively. Statistical significance is defined as follows: *, $p < 0.05$; **, $p < 0.01$. Data are expressed as mean of *n* experiments ± S.E.

the reconstituted actin-tropomyosin-myosin ATPase system in the presence of 1.0 mM EGTA in the absence of Ca^{2+} and decreased the ATPase activation in the same reconstituted system in the presence of maximal activating Ca^{2+}. Using skinned cardiac porcine muscle fibers reconstituted with hcTnI R145G, Lang *et al.* (14) concluded that there was an increase in the unregulated force in 10^{-8} M Ca^{2+} (also called basal force), a decrease in the maximal force recovery, a change in the Hill coefficient, and a significant increase in the Ca^{2+} sensitivity of force development when compared with the wild type hcTnI. These results suggested that diastolic and systolic dysfunction would be prominent clinical features of this mutation and might explain the cause of HCM and the poor prognosis seen in patients with these mutations.

In this study, the physiological changes caused by the hcTnI R145G mutation in transgenic mouse fibers were as follows. 1) There was a large increase in Ca^{2+} sensitivity of force development and ATPase activity (especially in the low activating range of Ca^{2+}) as well as a significant decrease in the Hill coefficient of force (Fig. 3). 2) There was a significant decrease in the maximal Ca^{2+}-activated force but no change in the maximal Ca^{2+}-activated ATPase (Fig. 4*a*). 3) There was no significant difference in the fraction of cross-bridges attached at maximum Ca^{2+} in all groups of fibers (Fig. 5). 4) The rate of cross-bridge turnover as a function of activation state (fraction of maximum activated force) was unchanged in Tg-R145G fibers compared with Tg-WT fibers (Fig. 6). 5) Energy cost (ATPase/force) as a function of active state was higher in Tg-R145G fibers than in Tg-WT fibers (Fig. 7). 6) In the presence of 10^{-9} M Ca^{2+}, ~2–4% of the force generating cross-bridges remained attached in the Tg-R145G fibers compared with less than 1.0% in Tg-WT fibers, suggesting that the hcTnI R145G mutation does not allow the complete inhibition of force-generating cross-bridges under relaxing conditions (Fig. 8). 7) Both force and intracellular Ca^{2+} transients were prolonged, with the force transient prolongation being more pronounced than in the Ca^{2+} transient (Fig. 9).

The significant decrease in the maximum Ca^{2+}-activated force in transgenic mice expressing hcTnI R145G (in this study), transgenic mice expressing mcTnI R146G (21), and reconstituted porcine skinned fibers (14) could be explained by a change in the cross-bridge kinetics or a decrease in the average force per cross-bridge, since the maximum force a fiber can generate is equal to the number of cross-bridges attached at maximum Ca^{2+} activation times the average force/cross-bridge (32). Using simultaneous measurements of force and ATPase activity in the transgenic skinned fibers in this study, it was found that a significant 14% decrease in maximum Ca^{2+}-activated force in Tg-R145G fibers was due to the decrease in the average force per cross-bridge rather than a change in cross-bridge kinetics, because the cross-bridge turnover rate (*g*) did not change. This means the Tg-R145G muscle would have to use more ATP to exert the same force as the Tg-WT muscle. This is also consistent with our result that Tg-R145G fibers have higher energy costs compared with Tg-WT fibers, as shown in Fig. 7. This fact alone may cause the R145G heart to hypertrophy in humans, because it would be equivalent to causing a WT muscle to work at a higher rate, as, for example, during exercise. It is well known that exercise can cause cardiac muscle to hypertrophy in humans (39).

As can be seen in Fig. 3, there was a large increase in Ca^{2+} sensitivity in the low range of Ca^{2+} activation. Also very noticeable in Fig. 3, there was a large decrease in the slope of the force-*p*Ca curve showing a decrease in the cooperative protein-protein interactions within the thin filament during activation

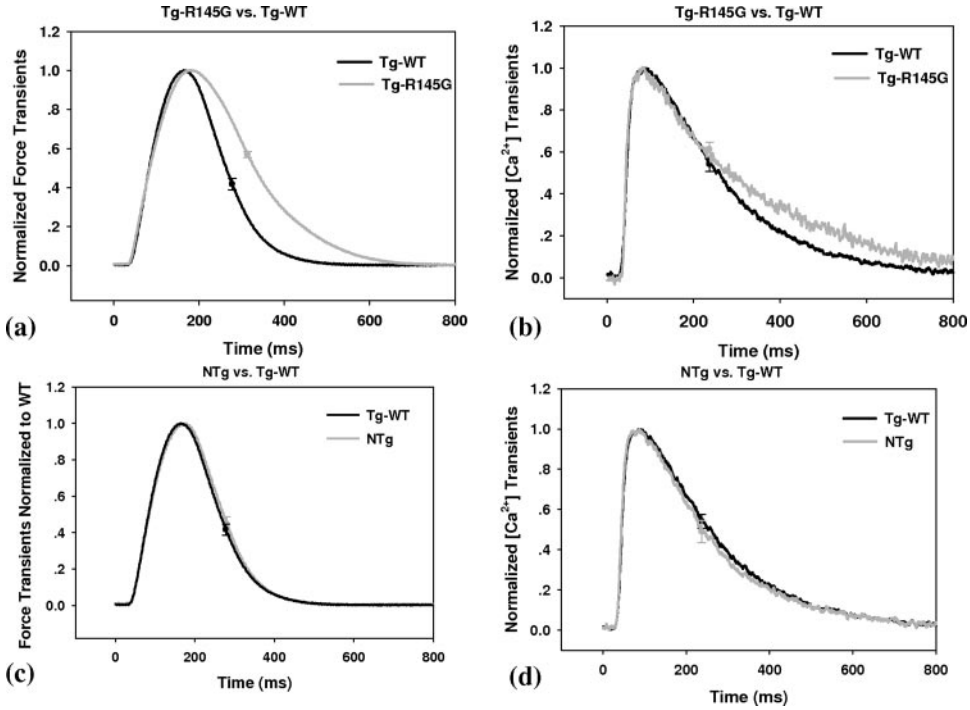

FIGURE 9. **Force and Ca^{2+} transients in intact transgenic papillary muscle fibers.** Shown are force (*a*) and $[Ca^{2+}]$ (*b*) transients in Tg-R145G ($n = 9$) *versus* Tg-WT ($n = 9$) intact papillary fibers. Also shown are force (*c*) and $[Ca^{2+}]$ (*d*) transients in NTg ($n = 5$) *versus* Tg-WT intact papillary fibers. Intact papillary muscle fibers were stimulated at 1.0 HZ. Fluorescence produced by Fura-2 was recorded at the same time (see "Materials and Methods" for details). As shown, force and $[Ca^{2+}]$ transients are both prolonged in Tg-R145G fibers compared with Tg-WT fibers. As predicted, force and $[Ca^{2+}]$ transients do not have significant difference in Tg-WT fibers compared with NTg fibers. Data are expressed as the mean of *n* ($n = 5$–9) experiments ± S.E.

TABLE 2

Force and $[Ca^{2+}]$ transients in NTg, Tg-WT, and Tg-R145G intact papillary fibers

$t_{50\ (duration)}$ is the time from peak to 50% of force or Ca^{2+} in relaxation; $t_{10(duration)}$ is the time from peak to 10% of force or Ca^{2+} in relaxation. Data are the mean of the *n* experiments ± S.E.

Mouse	Force transients		Ca^{2+} transients		*n*
	$t_{50(duration)}$	$t_{10(duration)}$	$t_{50(duration)}$	$t_{10(duration)}$	
	ms	*ms*	*ms*	*ms*	
NTg	79.0 ± 4.4	164.0 ± 12.4	165.8 ± 12.4	432.6 ± 9.3	5
Tg-WT	85.3 ± 4.3	180.4 ± 12.2	167.7 ± 6.8	489.7 ± 15.3	9
Tg-R145G	146.9 ± 9.0[a]	361.3 ± 13.3[a]	215.2 ± 5.0[a]	627.8 ± 13.4[a]	9

[a] Significantly different compared with Tg-WT and NTg ($p < 0.05$). There are no significant differences between Tg-WT and NTg.

that is known to be responsible for the steepness of muscle force-*p*Ca relationship. The decrease in the n_H indicated that the hcTnI R145G mutation might interfere with the Ca^{2+} effects of the nearest neighbor regulatory or cross-bridge binding to the nearest neighbor regulatory units. Previous cTn mutations related to HCM have been reported by our laboratories to cause changes in cooperativity of the thin filament, but the mechanism by which they cause these changes is still poorly understood (40, 41). These results lead us to the following question. What is responsible for the increase in Ca^{2+} sensitivity? There are two major possibilities: 1) a decrease in the cross-bridge turnover rate (42) and 2) a decrease in the off-rate of Ca^{2+} from the cardiac troponin C (29, 43). No change in cross-bridge turnover rate was observed (as shown in Fig. 6); thus, it is reasonable that the off rate of Ca^{2+} from cTnC was changed by the hcTnI R145G mutation. It is well known that TnI binding to TnC decreases the off rate of Ca^{2+} from TnC (6, 44). Our results are also in accordance with previous fluorescence data showing that this specific mutation leads to an increase in the Ca^{2+} affinity for cTnC in reconstituted thin filaments (45). This increase in Ca^{2+} sensitivity, especially in the low range of activating Ca^{2+}, is probably responsible for the prolongation of the Ca^{2+} and force transients observed in the intact papillary muscle (Fig. 9). This is because cardiac TnC is one of many Ca^{2+} buffers in the cardiac muscle myoplasm and thereby influences Ca^{2+} uptake by the sarcoplasmic reticulum during the relaxation phase of muscle contraction. Thus, a decrease in the off rate of Ca^{2+} from troponin C would lead to prolonging the Ca^{2+} and force transients as predicted by a computer model in Lang *et al.* (14).

The relative force due to 10–40% stretch of the fiber length under relaxing conditions (*p*Ca 9.0) in Tg-R145G skinned papillary fibers was shown to be slightly increased compared with the Tg-WT (Fig. 8*b*). In the presence of BDM, the Tg-R145G force-stretch curve shifts downward to superimpose with the Tg-WT force-stretch curve. This shows that there is active cross-bridge attachment that is responsible for the separation of the two force-stretch curves and is expected based on the incomplete inhibition of force and ATPase activity seen previously (14). As shown in Fig. 8*c*, Tg-R145G had 2–4 times more cross-bridges attached than that in the Tg-WT fibers under resting conditions. In agreement with Kruger *et al.* (13) and Lang *et al.* (14), our hcTnI transgenic mice results suggest that under relaxing conditions, the hcTnI R145G mutation impairs the inhibition of the actomyosin cross-bridge cycling.

As can be seen, the hcTnI R145G mutation causes three problems, all of which would be expected to adversely affect contractility. The first problem is a decrease in the average force per cross-bridge, resulting in a decrease in the force per cross-sectional area of ventricular muscle, which would cause a decreased stroke volume in R145G hearts under stress. The second problem is an increase in the Ca^{2+} sensitivity of force, probably due to a decrease in the Ca^{2+} off-rate from cTnC. This results in prolonged force and Ca^{2+} transients, which cause an increased resistance to filling the ventricle during diastole, especially at high heart rates. The third problem is an incomplete inhibition of cross-bridge attachment at 10^{-9} M Ca^{2+}. This would also result in an increase in resistance to filling the ventricle during diastole. These effects on diastolic filling (preload) would result in a decreased stroke volume (sv), especially under stress.

These three physiological effects of the hcTnI R145G mutation would cause the cardiovascular system to react by increas-

ing the heart rate (HR) to maintain a constant cardiac output (CO) (CO = HR × SV). From the muscle's point of view, energy cost (ATP hydrolysis) would increase because of this high heart rate as it does during exercise. Over time, a compensatory increase in muscle mass (hypertrophy) would substitute for the increase in heart rate in order to maintain cardiac output constant. Thus, all of the above physiological changes caused by the hcTnI R145G mutation would be predicted to be prohypertrophic in humans.

In summary, the hcTnI R145G mutation decreases the average force per cross-bridge, increases Ca^{2+} sensitivity in the low activating range of Ca^{2+}, impairs the cTnI ability to inhibit cross-bridge attachment under relaxing conditions, and prolongs force and intracellular Ca^{2+} transients. These physiological changes give insights into how the hcTnI R145G mutation might trigger hypertrophy and also into the poor prognosis of patients with this HCM mutation.

REFERENCES

1. World Health Organization/International Society and Federation of Cardiology Task Force (1980) *Br. Heart J.* **44,** 672–673
2. Marian, A. J., and Roberts, R. (1998) *J. Cardiovasc. Electrophysiol.* **9,** 88–99
3. Seidman, J. G., and Seidman, C. (2001) *Cell* **104,** 557–567
4. Fatkin, D., McConnell, B. K., Mudd, J. O., Semsarian, C., Moskowitz, I. G., Schoen, F. J., Giewat, M., Seidman, C. E., and Seidman, J. G. (2000) *J. Clin. Invest.* **106,** 1351–1359
5. Gomes, A. V., and Potter, J. D. (2004) *Ann. N. Y. Acad. Sci.* **1015,** 214–224
6. Solaro, R. J., and Rarick, H. M. (1998) *Circ. Res.* **83,** 471–480
7. Potter, J. D., and Gergely, J. (1974) *Biochemistry* **13,** 2697–2703
8. Kimura, A., Harada, H., Park, J. E., Nishi, H., Satoh, M., Takahashi, M., Hiroi, S., Sasaoka, T., Ohbuchi, N., Nakamura, T., Koyanagi, T., Hwang, T. H., Choo, J. A., Chung, K. S., Hasegawa, A., Nagai, R., Okazaki, O., Nakamura, H., Matsuzaki, M., Sakamoto, T., Toshima, H., Koga, Y., Imaizumi, T., and Sasazuki, T. (1997) *Nat. Genet.* **16,** 379–382
9. Richard, P., Charron, P., Carrier, L., Ledeuil, C., Cheav, T., Pichereau, C., Benaiche, A., Isnard, R., Dubourg, O., Burban, M., Gueffet, J. P., Millaire, A., Desnos, M., Schwartz, K., Hainque, B., and Komajda, M. (2003) *Circulation* **107,** 2227–2232
10. Van Driest, S. L., Ellsworth, E. G., Ommen, S. R., Tajik, A. J., Gersh, B. J., and Ackerman, M. J. (2003) *Circulation* **108,** 445–451
11. Kokado, H., Shimizu, M., Yoshio, H., Ino, H., Okeie, K., Emoto, Y., Matsuyama, T., Yamaguchi, M., Yasuda, T., Fujino, N., Ito, H., and Mabuchi, H. (2000) *Circulation* **102,** 663–669
12. Morner, S., Richard, P., Kazzam, E., Hainque, B., Schwartz, K., and Waldenstrom, A. (2000) *J. Mol. Cell Cardiol.* **32,** 521–525
13. Kruger, M., Zittrich, S., Redwood, C., Blaudeck, N., James, J., Robbins, J., Pfitzer, G., and Stehle, R. (2005) *J. Physiol.* **564,** 347–357
14. Lang, R., Gomes, A. V., Zhao, J., Housmans, P. R., Miller, T., and Potter, J. D. (2002) *J. Biol. Chem.* **277,** 11670–11678
15. Elliott, K., Watkins, H., and Redwood, C. S. (2000) *J. Biol. Chem.* **275,** 22069–22074
16. Takahashi-Yanaga, F., Morimoto, S., Harada, K., Minakami, R., Shiraishi, F., Ohta, M., Lu, Q. W., Sasaguri, T., and Ohtsuki, I. (2001) *J. Mol. Cell Cardiol.* **33,** 2095–2107
17. Burton, D., Abdulrazzak, H., Knott, A., Elliott, K., Redwood, C., Watkins, H., Marston, S., and Ashley, C. (2002) *Biochem. J.* **362,** 443–451
18. Westfall, M. V., Borton, A. R., Albayya, F. P., and Metzger, J. M. (2002) *Circ. Res.* **91,** 525–531
19. Kohler, J., Chen, Y., Brenner, B., Gordon, A. M., Kraft, T., Martyn, D. A., Regnier, M., Rivera, A. J., Wang, C. K., and Chase, P. B. (2003) *Physiol. Genomics* **14,** 117–128
20. Takahashi-Yanaga, F., Morimoto, S., and Ohtsuki, I. (2000) *J. Biochem.* (*Tokyo*) **127,** 355–357
21. James, J., Zhang, Y., Osinska, H., Sanbe, A., Klevitsky, R., Hewett, T. E., and Robbins, J. (2000) *Circ. Res.* **87,** 805–811
22. Sanbe, A., James, J., Tuzcu, V., Nas, S., Martin, L., Gulick, J., Osinska, H., Sakthivel, S., Klevitsky, R., Ginsburg, K. S., Bers, D. M., Zinman, B., Lakatta, E. G., and Robbins, J. (2005) *Circulation* **111,** 2330–2338
23. Ausubel, F. M., Kingston, R. E., Moore, D. D., Seidman, J. G., Smith, J. A., and Struhl, K. (1995) in *Current Protocols in Molecular Biology*, Vol. 1, chapter 8, John Wiley & Sons, Inc., New York
24. Brinster, R. L., Chen, H. Y., Trumbauer, M. E., Yagle, M. K., and Palmiter, R. D. (1985) *Proc. Natl. Acad. Sci. U. S. A.* **82,** 4438–4442
25. Donaldson, S. K., and Kerrick, W. G. (1975) *J. Gen. Physiol.* **66,** 427–444
26. Allen, K., Xu, Y. Y., and Kerrick, W. G. (2000) *J. Appl. Physiol.* **88,** 180–185
27. Guth, K., and Wojciechowski, R. (1986) *Pflügers Arch. Eur. J. Physiol.* **407,** 552–557
28. Hernandez, O. M., Szczesna-Cordary, D., Knollmann, B. C., Miller, T., Bell, M., Zhao, J., Sirenko, S. G., Diaz, Z., Guzman, G., Xu, Y., Wang, Y., Kerrick, W. G., and Potter, J. D. (2005) *J. Biol. Chem.* **280,** 37183–37194
29. Wang, Y., Xu, Y., Guth, K., and Kerrick, W. G. (1999) *J. Muscle Res. Cell Motil.* **20,** 645–653
30. Ward, C. W., Williams, J. H., and Kerrick, W. G. L. (2004) *J. Biol. Chem.* **280,** 37183–37194
31. Takashi, R., and Putnam, S. (1979) *Anal. Biochem.* **92,** 375–382
32. Kerrick, W. G., and Xu, Y. (2004) *J. Muscle Res. Cell Motil.* **25,** 107–117
33. Ferenczi, M. A., Homsher, E., and Trentham, D. R. (1984) *J. Physiol.* **352,** 575–599
34. Wang, Y., Xu, Y., Kerrick, W. G., Wang, Y., Guzman, G., Diaz-Perez, Z., and Szczesna-Cordary, D. (2006) *J. Mol. Biol.* **361,** 286–299
35. Ng, W. A., Grupp, I. L., Subramaniam, A., and Robbins, J. (1991) *Circ. Res.* **68,** 1742–1750
36. Sinha, A. M., Umeda, P. K., Kavinsky, C. J., Rajamanickam, C., Hsu, H. J., Jakovcic, S., and Rabinowitz, M. (1982) *Proc. Natl. Acad. Sci. U. S. A.* **79,** 5847–5851
37. Krenz, M., and Robbins, J. (2004) *J. Am. Coll. Cardiol.* **44,** 2390–2397
38. Herron, T. J., Vandenboom, R., Fomicheva, E., Mundada, L., Edwards, T., and Metzger, J. M. (2007) *Circ. Res.* **100,** 1182–1190
39. Abergel, E., and Oblak, A. (2006) *Arch. Mal. Coeur Vaiss.* **99,** 969–974
40. Szczesna, D., Zhang, R., Zhao, J., Jones, M., Guzman, G., and Potter, J. D. (2000) *J. Biol. Chem.* **275,** 624–630
41. Harada, K., and Potter, J. D. (2004) *J. Biol. Chem.* **279,** 14488–14495
42. Robinson, J. M., Wang, Y., Kerrick, W. G., Kawai, R., and Cheung, H. C. (2002) *J. Mol. Biol.* **322,** 1065–1088
43. Wang, Y., and Kerrick, W. G. (2002) *J. Appl. Physiol.* **92,** 2409–2418
44. Johnson, J. D., Collins, J. H., Robertson, S. P., and Potter, J. D. (1980) *J. Biol. Chem.* **255,** 9635–9640
45. Kobayashi, T., and Solaro, R. J. (2006) *J. Biol. Chem.* **281,** 13471–13477